Published in final edited form as:
Immunity. 2010 November 24; 33(5): 817–829. doi:10.1016/j.immuni.2010.10.018.

Endothelial Heparan Sulfate Controls Chemokine Presentation in Recruitment of Lymphocytes and Dendritic Cells to Lymph Nodes

Xingfeng Bao[1], **E. Ashley Moseman**[2], **Hideo Saito**[1,4], **Bronislawa Petryanik**[3,4], **Aude Thiriot**[2], **Shingo Hatakeyama**[1,4], **Yuki Ito**[1], **Hiroto Kawashima**[1,4], **Yu Yamaguchi**[1,5], **John B Lowe**[3,4], **Ulrich H von Andrian**[2], and **Minoru Fukuda**[1,*]

[1] Glycobiology Unit, Sanford-Burnham Medical Research Institute, La Jolla, California 92037, USA

[2] Department of Pathology, Harvard Medical School, Boston, Massachusetts 02115, USA

[3] Department of Pathology, Case Western Reserve University School of Medicine, Cleveland, Ohio 44106, USA

[5] Sanford Children's Health Research Center, Sanford-Burnham Medical Research Institute, La Jolla, California 92037, USA

SUMMARY

Heparan sulfate can bind several adhesion molecules involved in lymphocyte trafficking. However, the *in vivo* function of endothelial heparan sulfate in lymphocyte homing and stimulation of the immune response has not been elucidated. Here, we generated mutant mice deficient in the enzyme Ext1, which is required for heparan sulfate synthesis, in a *Tek*-dependent and inducible manner. Chemokine presentation was diminished in the mutant mice, causing the lack of appropriate integrin-mediated adhesion, and resulted in a marked decrease in lymphocyte sticking to high endothelial venules and in recruitment of resident dendritic cells through lymphatic vessels to the lymph nodes. As a consequence, mutant mice displayed a severe impairment in lymphocyte homing and a compromised contact hypersensitivity response. By contrast, lymphocyte rolling was increased due to loss of electrostatic repulsion by heparan sulfate. These results demonstrate critical roles of endothelial heparan sulfate in immune surveillance and immune response generation.

INTRODUCTION

Immune surveillance requires continuous recruitment of both lymphocytes from blood circulation and antigen presenting cells from peripheral tissues to lymph nodes, where they can interact in order to initiate an adaptive immune response (Butcher and Picker, 1996;

[*]Corresponding should be addressed to M.F. (minoru@burnham.org).
[4]Present address: Tohoku University School of Medicine, Sendai, 980-8574 Japan (H.S.); Genentech, South San Francisco, CA94080, USA (B.P., J.B.L); Hirosaki University School of Medicine, Hirosaki, 036-8562 Japan (S.H.); School of Pharmaceutical Sciences, University of Shizuoka, Shizuoka, 422-8526 Japan (H.K.).

SUPPLEMENTAL INFORMATION
Supplemental Information includes Supplemental Experimental Procedures, seven Figures and one Table.

Marchesi and Gowans, 1964). Dendritic cells and other antigen presenting cells enter lymph nodes through afferent lymphoid vessels, while lymphocytes enter lymph nodes through a specialized vasculature of high endothelial venules (HEVs). Homing of lymphocytes to lymph nodes involves multiple stepwise interactions between lymphocytes and HEV cells, including L-selectin-mediated cell rolling and tethering, chemokine-mediated integrin activation, and integrin-mediated cell sticking or firm adhesion, which leads to transmigration across blood vessels (McEver and Zhu, 2010; Rosen, 2004; Springer, 1994; von Andrian and Mempel, 2003).

Molecular and cell-based studies indicate that heparan sulfate binds *in vitro* to several major molecules including L-selectin, chemokines and integrins involved in lymphocyte homing (Parish, 2006). In HEV, we and others have demonstrated that a specialized carbohydrate termed 6-sulfo sialyl Lewis X (sialic acidα2→3Galβ1→4[Fucα1→3(sulfo→6)]GlcNAc, 6-sulfo sLeX), is the functional ligands for L-selectin by analyses of mutant mice deficient in fucosyltransferase (FucT) IV and VII (Homeister et al., 2001), core 2 *N*-acetylglucosaminyltransferase (GnT)-1 (Ellies et al., 1998; Yeh et al., 2001), *N*-acetylglucosamine-6-*O*-sulfotransferases (GlcNAc6ST) -1 and -2 (Kawashima et al., 2005; Uchimura et al., 2005), and core 1 β3GnT and core 2 GnT-1 (Mitoma et al., 2007). However, sulfation of heparan sulfate in lung endothelial cells was recently reported to modulate L-selectin binding and L-selectin-mediated cell rolling in lung microcapillaries (Wang et al., 2005). Thus, the *in vivo* contribution of endothelial heparan sulfate in L-selectin-mediated lymphocyte rolling during lymphocyte homing remains obscure.

Most chemokines, including the secondary lymphoid chemokine CCL21 (also called SLC), which is indispensable for lymphocyte homing, bind *in vitro* to heparan sulfate or its highly sulfated analog heparin (Lortat-Jacob et al., 2002). Heparan sulfate-bound chemokines are recognized by chemokine receptors such as CCR6 and CCR7, thereby activating integrins leading to lymphocyte extravasation (von Andrian and Mempel, 2003). Multiple lines of evidence indicate that heparan sulfate functions in transcytosis, presentation, and gradient formation of chemokines to promote lymphocyte migration (Lander et al., 2002; Middleton et al., 1997). Studies utilizing *in vitro* flow chamber models have shown that under shear flow, the cell-bound chemokine (CCL21) but not soluble CCL19 activate integrins on rolling lymphocytes to allow interaction with its ligand, intercellular adhesion molecule 1 (ICAM-1) (Shamri et al., 2005). However, the physiological role of HEV heparan sulfate in the chemokine-mediated lymphocyte homing has not been determined.

Recruitment of antigen-bearing dendritic cells from peripheral tissues to lymph nodes is crucial for adaptive immune response generation. The migration of dendritic cells is directed by both the cell-bound chemokine CCL21 and the soluble chemokine CCL19, which form a gradient in the intestinal tissue to guide the tissue resident dendritic cells to move towards draining lymph nodes *via* lymphatic vessels (Bajenoff et al., 2006; Schumann et al., 2010). It is not known whether heparan sulfate, in particular lymphatic endothelial heparan sulfate, plays a role in this process.

To examine the pathophysiological functions of endothelial heparan sulfate in the recruitment of lymphocytes and dendritic cells to lymph nodes, we first inactivated the exostoses-1 (*Ext1*) gene, which is required for the formation of heparan sulfate chains, in a *Tek*-dependent manner, but homozygous mice died before birth. To bypass the embryonic lethality, we generated transgenic mice harboring a tetracycline-controlled transactivator (rtTA) gene under *Tek* promotor (*Tek-rtTA*) and inactivated *Ext1* in a *Tek*-dependent and inducible manner. Using this mouse model, we demonstrate in this study that heparan sulfate is critically required for chemokine immobilization and functional presentation on the cell surface of both HEV cells and lymphatic endothelial cells. Removal of endothelial heparan

sulfate diminishes lymphocyte sticking during lymphocyte homing and decreases recruitment of dendritic cells *via* lymphatics to lymph node, which leads to a compromised response in contact hypersensitivity. We also found that endothelial heparan sulfate antagonizes L-selectin-counterreceptor interactions in HEV thus attenuating lymphocyte rolling. These results establish crucial but multifaceted functions of endothelial heparan sulfate in lymphocyte homing and dendritic cell recruitment, and thereby immune response generation.

RESULTS

Enzymatic Removal of Endothelial Heparan Sulfate Diminishes Lymphocyte Homing

To assess the *in vivo* function of HEV heparan sulfate in lymphocyte homing, we infused a mixture of heparitinase and heparinase (hereafter, "HSases" is used) to wild-type (WT) mice through the tail veins to enzymatically remove the endothelial heparan sulfate in HEV. Lymphocyte homing to both peripheral lymph nodes (PLNs) and mesenteric lymph nodes (MLNs) of the HSase-infused mice was significantly decreased compared with those of PBS-infused mice (Figure 1A), Less than 20% of homing activity to PLNs was detected in HSase-infused mice. No decrease, but rather a slight increase in homing was found for those infused with chondroitinase ABC (CSase ABC) (Figure 1A), which degrades chondroitin sulfate and dermatan sulfate in addition to hyaluronic acid. In these assays, either HSases or CSase ABC specifically degraded their respective glycosaminoglycans on both the luminal surface and subcellular matrix of lymph node HEV endothelial cells (Figure 1B). By contrast, treatment of lymphocytes with HSases had no effect at all in the homing to lymph nodes (Figure 1C). These results demonstrated a specific and critical role of heparan sulfate on HEV in the homing of lymphocytes to lymph nodes.

Antigen MECA-79$^+$ lymph node HEV cells express two major membrane heparan sulfate proteoglycans (PGs), syndecan-4 and glypican-1, and a minor proteoglycan syndecan-2 (Figure 1D). Immunoblotting confirmed the predominant expression of syndecan-4 and glypican-1 in lymph node HEV (Figure 1E). However, we detected no alteration in the lymph node cellularity and lymphocyte homing in the syndecan-4 deficient mice (Ishiguro et al., 2000) compared to WT mice (data not shown). These results indicate that multiple heparan sulfate PGs in lymph node HEV cells collectively contribute to regulation of lymphocyte homing.

Conditional Inactivation of *Ext1* in an Inducible Manner

To determine the physiological function of endothelial heparan sulfate in immune surveillance and chronic inflammation, we initially crossbred *Tek-Cre* mice (Koni et al., 2001) with *Ext1*$^{flox/flox}$ mice (Inatani et al., 2003) to delete *Ext1* in endothelial cells. No such conditional homozygous mice were born indicating an embryonic lethality of the conditionally ablated mice (data not shown). To bypass embryonic lethality, we used a Tet-on system-based inducible targeting approach to inactivate *Ext1* in endothelial cells and leukocytes only at adult stage by crossbreeding of *Tek-rtTA* mice, *Tet-Cre* mice (Belteki et al., 2005) and *Ext1*$^{flox/flox}$ mice. To generate *Tek-rtTA* transgenic mice, we made a transgenic vector containing the mouse *Tek* promoter (Schlaeger et al., 1997), *rtTA* with a poly A sequence, and the full length mouse *Tek* enhancer (Figure S1A, B). Among 9 transgenic mouse clones with *Tek-rtTA* gene (Figure S1C), two independent transgenic clones (#8 and #29) exhibited identical specificity and effectiveness in β-galactosidase recombination in *Rosa26r* reporter mice (Figure S2), and the #29 mouse line was used hereafter. Whole mount staining for β-galactosidase by X-gal solution of the intercrosses of *Tek-rtTA, Tet-Cre* and *Rosa*$^{flox/flox}$ (*Tek-rtTA*$^+$*:Tet-Cre*$^+$*:Rosa*$^{flox/wt}$) with or without 2 weeks of doxycycline (Dox) treatment through drinking water, indicated that the vasculature, lymphocytes, and

hematopoietic cells of the heart, lung, aorta and lymph nodes were positive, which is consistent with the reported expression profile of the *Tek* gene (Koni et al., 2001). By contrast, those of *Tek-rtTA*$^{+}$*:Tet-Cre*$^{-}$*:Rosa*$^{flox/wt}$ were negative (Figure S2). Notably, some vasculatures in the lung and lymphocytes in the lymph nodes of the *Tek-rtTA*$^{+}$*:Tet-Cre*$^{+}$*:Rosa*$^{flox/wt}$ without Dox treatment are weak positive for X-gal indicating a baseline, Dox-independent expression in the system.

To inactivate heparan sulfate synthesis, *Tek-rtTA*$^{+}$*:Tet-Cre*$^{+}$*:Ext1*$^{flox/wt}$ mice were further crossbred with *Ext1*$^{flox/flox}$ mice to generate *Tek-rtTA*$^{+}$*:Tet-Cre*$^{+}$*:Ext1*$^{flox/flox}$ mice (Figure S1A). These mice were born and thrived normally and showed no overall difference from their control *Tek-rtTA*$^{+}$*:Tet-Cre*$^{-}$*:Ext1*$^{flox/flox}$ and *Tek-rtTA*$^{-}$*:Tet-Cre*$^{-}$*:Ext1*$^{flox/flox}$ littermates. Dox administration of 1 month old mice brought a gradual loss of heparan sulfate in lymph node HEV of *Tek-rtTA*$^{+}$*:Tet-Cre*$^{+}$*:Ext1*$^{flox/flox}$ (mutant mice), while no change was detected for the similar Dox-treated control mice (Figure S3A).

After a 3 week treatment with Dox, heparan sulfate expression was barely detectable in the HEV of mutant mice, while CD31^{+} vasculatures and core protein of the basement membrane heparan sulfate PG, perlecan, were both distributed normally in the lymph nodes (Figure 2A and Figure S3A). Polymerase chain reaction (PCR) analyses of freshly isolated MECA-79^{+} lymph node HEV cells from mutant mice showed minimal levels of *Ext1* mRNA and robust signals for inactivated *Ext1* (Figure 2B). As expected from the X-gal staining, a low level of genomic *Ext1* deletion was seen in cells of the mice that received no Dox (Figure 2B). Immunoblotting analysis of isolated CD31^{+} lung pan-endothelial cells showed a reduced molecular size of syndecan-4 in mutant mice (Figure 2C). The size was not altered by further treatment with HSases, but treatment with both HSases and CSase ABC resulted in further reduction of syndecan-4 size to about 35 kda (Figure 2C). Enzyme-linked immunosorbent assay (ELISA) showed that approximately 90% of heparan sulfate on syndecan-4 in lung pan-endothelial cells was lost in the mutant mice compared to control mice (Figure 2D). In addition, consistent with the X-gal staining, a similar deletion profile of *Ext1* gene in splenic lymphocytes of mutant mice was also detected (Figure S3B, C).

Overall, these results indicate that we have generated an *in vivo* recombination system, which specifically and efficiently deletes virtually all heparan sulfate in endothelial cells including lymph node HEV in adult mice. To our knowledge, this is the first live animal model that lose endothelial heparan sulfate.

Diminished Lymphocyte Homing and Cell Sticking in HEV of *Ext1* Mutant Mice Due to Diminished Chemokine Presentation

After three weeks of Dox treatment, mutant mice showed no gross abnormalities, but cell numbers of PLN, MLN and PP (Peyer's Patches) were all about 50% lower than those of control mice (Figure 3A). By contrast, the numbers of lymphocytes and granulocytes in the peripheral blood are increased (Figure 3B), similar to that observed in FucT-IV$^{-/-}$:FucT-VII$^{-/-}$ mice (Homeister et al., 2001). Lymph node cellularity was further reduced after a two month treatment with Dox and the gross sizes of PLNs were smaller than those of control mice (Figure 3C insert). This difference in the cell number was not due to an altered cell proliferation based on *in vitro* assessment by using mitogen concanavalin A (Figure 3D), a finding consistent with a previous report that T- or B-cell specific deletion of heparan sulfate does not alter T and B cell proliferation (Garner et al., 2008). Both T cells and B cells appeared similarly affected (Figure 3E). In line with the reduced cellularity, homing of lymphocytes to PLN, MLN and PP was all significantly decreased (Figure 3F). The remaining one-third of homing activity in PLNs of mutant mice was further reduced to background amounts by a tail vein infusion of HSases (Figure 3F, left panels), whereas a slightly increased homing to spleen was detected in mutant mice (Figure 3F, right panels).

On the other hand, lymphocytes isolated from control and mutant mice had the same capability of homing to wild-type lymph nodes (Figure 3G), indicating that *Ext1* gene abrogation in lymphocytes has no effect on their homing activity. The spatial distribution of T and B cells in the lymph nodes in the mutant mice was also normal (Figure 3H). These results together demonstrate that endothelial heparan sulfate but not lymphocyte heparan sulfate plays a decisive role in lymphocyte homing.

Intravital microscopic analysis showed a reduced sticking of T lymphocytes in typical lymph node HEV order III venules (M'Rini et al., 2003) of the mutant mice when compared to that of control mice (Figure 4A). This situation was similar to pertussis toxin-treated mice (Warnock et al., 1998). Under the same conditions, only a slight increase in blood flow velocity was observed (V_{blood} in Table S1). The diminished lymphocyte sticking in order III venules was associated with the decrease of lymphocyte rolling velocity (Figure 4B, right panel), indicating that lymphocytes slowly kept rolling rather than arrest on endothelium in the absence of heparan sulfate. Loss of HEV heparan sulfate was accompanied by a loss of endothelial presentation of endogenous CCL21 and CCL2 (Figure 4C and Figure S4), but no alteration in the expressions of MECA-79 antigen, L-selectin ligands or ICAM-1 (Figure 4C) was observed. The little remaining CCL21 in the HEV of mutant mice could bind to the residual heparan sulfate and/or other molecules such as collagen IV (Yang et al., 2007). Heparan sulfate and CCL21 in the fibroblastic reticular network was not, however, affected in the mutant mice (Figure 4C and Figure S4B), suggesting a role of heparan sulfate synthesized by stromal cells in presenting CCL21 in the fibroblastic reticular network. CCL21 is a critical chemokine for lymphocyte homing (Nakano et al., 1998). CCR7 is the cognate receptor on lymphocytes for CCL21 (Forster et al., 1999). We found that homing of lymphocytes in $Ccr7^{+/-}$ mice to $Ext1^{+/-}$ mice lymph nodes was significantly lower than homing of lymphocytes in WT mice to the same $Ext1^{+/-}$ mouse lymph nodes or $Ccr7^{+/-}$ lymphocytes in WT mice (Figure 4D), indicating that HEV heparan sulfate is genetically connected to the CCL21-CCR7 signaling for lymphocyte homing. These results demonstrate that endothelial heparan sulfate plays an essential role in immobilization and presentation of chemokines including CCL21 and thereby in the regulation of lymphocyte sticking in lymph node HEV.

Increased Lymphocyte Rolling in HEV of Mutant Mice

Apart from the reduced lymphocyte sticking in mutant mice, we noticed reduced rolling velocity in MECA-79^{+} order III venules (Figure 4B) along with an increased rolling of T cells in order II venules (Figure 4E), suggesting that endothelial heparan sulfate negatively regulates L-selectin-mediated cell rolling. Order II venules are downstream from order III venules. It is thus possible that lymphocytes, which begin to roll in higher order venules (III, IV and V) yet fail to stick due to lack of heparan sulfate, may simply continue rolling through downstream orders, resulting in higher rolling fraction in order II venules without significant decrease in lymphocyte sticking (Figure 4A). Immunofluorescence staining showed indistinguishable expression of L-selectin ligands in HEV of control and mutant mice (Figure 4C). Analysis of splenic T and B cells also showed a normal expression of L-selectin at both mRNA and protein levels in mutant mice (Figures S3B, C). These results indicate that genetic removal of endothelial heparan sulfate had no effect in the expression of L-selectin in lymphocytes and of L-selectin ligands in HEV.

To delineate the effects of cell surface heparan sulfate in L-selectin-mediated lymphocyte rolling, we measured the rolling of 38C13 B cells (van Zante et al., 2003) on genetically engineered Chinese hamster ovary (CHO) cells, which mimic the glycan profile of HEV cells by stably expressing *O*- and *N*-glycan-based 6-sulfo sLeX (Mitoma et al., 2007) in a flow chamber before and after HSase and CSase ABC digestion (Figure S5C). These CHO cells supported the rolling of lymphocytes under shear flow, and the rolling was increased

after both heparan sulfate and chondroitin sulfate and dermatan sulfate or only heparan sulfate were removed (Figure 5A, B). In contrast, CHO cells expressing only CD34 and FucT-VII barely supported lymphocyte rolling and treatment with both HSase and CSase ABC had no effect on cell rolling (Figure 5A, B). Consistently, the rolling velocity on HSase-treated 6-sulfo sLeX-expressing cells decreased compared with PBS-treated cells (Figure 5C). Taking together, these *in vitro* and *in vivo* rolling data indicate that cell surface heparan sulfate does not function as L-selectin ligands to support cell rolling, but rather attenuates L-selectin binding to ligands, most likely due to electrostatic repulsion by sulfate groups.

Contact Hypersensitivity is Altered in Mutant Mice

The above findings suggest that lymphocyte recruitment in inflamed tissues may also depend on endothelial heparan sulfate. To test this hypothesis, we evaluated a contact hypersensitivity response, which is primarily mediated by T cells (Staite et al., 1996). Mutant mice showed significant reductions in ear swelling and in mononuclear cell infiltration after sensitization and challenge with the hapten DNFB (2,4-dinitrofluorobenzene; Figure 6A, B). The recruitment of $CD3^+$ T cells was substantially reduced in inflamed ears of the mutant mice (Figure 6C, left panels and Figure S6A). Analysis of draining lymph nodes after sensitization indicated that both total cell number and homing activity in the draining lymph nodes of mutant mice were lower than those of control mice (Figure 6D). Notably, the epidermal infiltration of neutrophils (Staite et al., 1996) was evident in inflamed control mouse ears, whereas such infiltration was significantly reduced in the mutant mice similar to P-selectin deficient mice (Subramanianm et al., 1995) (Figure 6C, right panel and Figure S6B). Consistent with decreased neutrophil infiltration, immobilization of CXCL-2, which regulates neutrophil recruitment in inflamed tissues, was diminished in the mutant mice (Figure 6E), while lymphocytes from both mouse lines proliferated at the same rate in response to 2,4-dinitrobenzene sulfonic acid (Figure 6F). These results suggest that significantly decreased recruitment of antigen-specific lymphocytes to the draining lymph nodes and reduced neutrophil recruitment to the inflamed ear collectively contributed to a reduced contact hypersensitivity response in mutant mice. By contrast, GlcNAc6ST-1 and -2 double deficient mice exhibited reduced recruitment of mononuclear cells but not of neutrophils (Figure S6C; Kawashima et al., 2005).

Dendritic Cell Homing During Inflammation is Impaired in Mutant Mice

To further study the mechanism of reduced contact hypersensitivity in mutant mice as shown above, we examined the migration of tissue resident dendritic cells to the draining lymph node, an earlier step ininitiating the adaptive immune response. Using a skin painting model, we found that the recruitment of $CD11c^+$ and $FITC^+$ double positive cells to the draining lymph nodes was significantly lower (one third reduction) in the mutant mice than the control mice (Figure 7A, left panel). Accordingly, the total cell number of draining lymph nodes was fewer in the mutant mice (Figure 7A, right panel). Endogenous dendritic cells in the inflamed skin of the mutant mice were not reduced as much as those in the wild-type mice (Figure 7B), indicating that recruitment of dendritic cells to the draining lymph nodes was impaired. However, the recruited $FITC^+$ cells appear to equally entered into the T cell zone of the draining lymph nodes of both mouse lines (Figure 7C), indicating that intranodal migration of recruited dendritic cells was normal in the mutant mice. We also assayed homing of exogenous bone marrow-derived dendritic cells to the draining lymph nodes under inflammatory condition stimulated by DNFB and detected an almost identical reduction of dendritic cell homing to the draining lymph nodes as seen after FITC-skin painting (Figure 7D). These results indicate that homing of not only lymphocytes *via* blood but also dendritic cells *via* lymphatics was impaired in the mutant mice.

Tek gene is known to be expressed in the lymphatic endothelial cells (Shimoda, 2009). In order to measure heparan sulfate of the lymphatic endothelial cells, we cultured dermal cells *in vitro* and isolated the podoplanin$^+$ lymphatic endothelial cells (Kriehuber et al., 2001) from the skin of control and mutant mice. Cells from both mouse lines grew similarly *in vitro*. Flow cytometric analysis showed a substantially lower expression of heparan sulfate assessed by antibody 10E4 in the lymphatic endothelial cells from the mutant mice compared with those of the control mice (Figure S7A). Cell-based ELISA demonstrated over an 80% reduction in heparan sulfate in lymphatic endothelial cells from the mutant mice (Figure 7E). Consequently, the binding capacity of the mutant cells toward the exogenous chemokines CCL21 and CCL19 was much lower than those of control mice (Figure 7F). Immunofluorescence analysis confirmed the diminished presentation of CCL21 in lymphatic vessels with a normal structural distribution in the DNFB-stimulated mutant mouse skin (Figure S7B, C).

These results collectively indicate that decreased expression of heparan sulfate in lymphatic endothelial cells reduces homing of tissue resident dendritic cells to draining lymph nodes in inflammatory conditions because of insufficient immobilization of chemokines required for dendritic cell recruitment to lymphatic vessels.

DISCUSSION

Recruitment of lymphocytes from blood circulation and dendritic cells from peripheral tissues to the lymph nodes is essential to maintain immune surveillance and generation of the adaptive immune response during inflammation. Here we have provided the *in vivo* evidence for the critical functions of endothelial heparan sulfate in the homing of both lymphocytes and dendritic cells to the lymph nodes under pathophysiological conditions by analyzing an inducible and conditional genetically targeted mouse model.

Lymphocyte homing is tightly controlled by three overlapping stepwise interactions between lymphocytes and HEV cells (Butcher and Picker, 1996; Springer, 1994). The initial rolling step is mediated by L-selectin on lymphocytes (Arbones et al., 1994), which binds to 6-sulfo sLeX and sLeX on HEV cells (Rosen, 2004). While heparan sulfate was shown to support L-selectin-mediated rolling of neutrophils in lung microcapillaries in acute inflammation (Wang et al., 2005), our current studies on genetic removal of HEV heparan sulfate did not decrease but increased the lymphocyte rolling *in vivo* and *in vitro*, demonstrating that endothelial heparan sulfate is not a L-selectin ligand in HEV. This conclusion is in line with the previous reports that sLeX or its 6-sulfated analogs are entirely responsible for the L-selectin-mediated lymphocyte homing (Homeister et al., 2001; Kawashima et al., 2005; Mitoma et al., 2007; Uchimura et al., 2005; Yeh et al., 2001). The distinct functions of endothelial heparan sulfate in the L-selectin-mediated leukocyte trafficking may be due to the availability of the potent L-selectin ligand 6-sulfo sLeX and sLeX in different recruitment sites.

Decreased cell rolling velocity after removal of heparan sulfate is a surprise considering normal expressions of L-selectin ligands in HEV and of L-selectin in lymphocytes in the mutant mice. Most L-selectin counter-receptors in HEV are mucin glycoproteins containing various numbers of *O*- and *N*-glycans (Rosen, 2004), which have a rod-like shape and extend outward from the cell membrane (Cyster et al., 1991). An extended form of L-selectin was also shown to enhance the adhesion under shear flow (Phan et al., 2006). In the same context, integrins on lymphocytes change from a bent conformation to an extended conformation after chemokine stimulation, thereby binding the adhesion molecule ICAM-1 on HEV cells (Shamri et al., 2005; Shimaoka et al., 2003). Thus, the adhesion molecules apparently favor the extended form when they interact with counterreceptors on opposing

cells (McEver and Zhu, 2010). Heparan sulfate PGs and chondroitin sulfate PGs are also extended molecules from the cell membrane with high negative charge density (Bishop et al., 2007) and may interfere with the interaction of L-selectin with 6-sulfo sLeXin HEV *via* steric hindrance. It will be of interest to examine whether glycosaminoglycans play a similar inhibitory role in regulating P-selectin- and PSGL-1-mediated cell rolling in peripheral blood vessels.

The firm adhesion of lymphocytes in lymph node HEV requires chemokine-mediated integrin activation. Our study is the first report to demonstrate the biological importance of HEV heparan sulfate in chemokine immobilization and functional presentation *in vivo*. The diminished lymphocyte sticking in HEV and reduced lymphocyte homing in mutant mice or HSase-infused mice provides direct evidence for this conclusion and is consistent with a previous report that heparan sulfate regulates the binding of cytokines CXCL1 and CXCL2 to lung microcapillary endothelial cells in vitro (Wang et al., 2005). Thus, HEV heparan sulfate possesses two opposite functions during lymphocyte homing: 1) negative regulation of L-selectin-mediated cell rolling; and 2) positive regulation of chemokine-mediated cell sticking, although the latter is the major one.

Our current studies demonstrate that heparan sulfate critically regulates the immobilization of chemokines on lymphatic endothelium and that the binding capacity of lymphatic endothelial cells for CCL19 is about half of that for CCL21. The lower binding capacity for CCL19 is consistent with a report showing a weak binding of CCL19 to heparan sulfate (de Paz et al., 2007). Since the heparinase treatment of lymphatic endothelium did not remove all the binding capacity of CCL19. As such, CCL19 might bind to other cell surface molecules in addition to heparan sulfate. CCL21 and CCL19 cause random movement and chemotactic movement respectively, and collaboration of both chemokines is necessary for dendritic cell migration to the lymph node (Schumann et al., 2010). Future studies will be significant to determine if the gradient of CCL19 is due to the gradient of heparan sulfate expression in the tissue and lymph node.

Our heparan sulfate mutant mice showed a phenotype of reduced homing of lymphocytes and dendritic cells, which is most reminiscent of the phenotype of *Ccr7*$^{-/-}$ mice (Forster et al., 1999) and CCL21 and CCL19 double-deficient *plt/plt* mice (Nakano et al., 1998). Our mice also displayed reduced infiltration of both mononuclear cells and neutrophils in the contact hypersensitivity assay. The reduced neutrophil infiltration in inflamed ears in the mutant mice was most likely due to an impaired presentation of relevant chemokines such as CXCL2 and impaired endothelial CXCL2 gradient formation required for the directed extravasation of neutrophils seen in a heparanase-expressing transgenic mice (Massena et al., 2010). On the other hand, we observed decreased recruitment of lymphocytes but not neutrophils in GlcNAc6ST-1 and -2 double deficient mice, while lymphocyte recruitment to the lymph nodes was only marginally affected in P- and E-selectin double deficient mice (Staite et al., 1996). The phenotypes of our mutant mice in pathophysiological conditions indicate that endothelial heparan sulfate participates in the recruitment of different types of leukocytes both from the blood circulation into lymph nodes and from inflammatory sites into draining lymph nodes.

Our studies showed that genetic deletion of a major heparan sulfate PG of HEV, syndecan-4, has essentially no effect in lymphocyte homing. This finding is consistent with the reports showing that genetic deletion of one of L-selectin counterreceptors such as GlyCAM-1 had a minimal effect on lymphocyte homing (Kansas, 1996). By contrast, genetic abrogation of 6-sulfo sialyl Lewis X had profound effect on lymphocyte homing (Homeister et al., 2001; Kawashima et al., 2005; Mitoma et al., 2007; Uchimura et al., 2005). Taken together with the present study, these observations illustrate that the functionality of L-selectin

counterreceptors and heparan sulfate PGs are largely dependent on their specific functional glycans.

In summary, our results have demonstrated critical functions of endothelial heparan sulfate in the recruitment of lymphocyte and dendritic cells to lymph nodes under both physiological and inflammatory conditions. We thus propose endothelial heparan sulfate as a drug target for attenuating chronic inflammation. The unique animal model reported here will be useful for studying the roles of heparan sulfates in inflammatory diseases such as asthma and inflammatory bowl diseases, and tumor angiogenesis.

EXPERIMENTAL PROCEDURES

Mice

All mice used in the study were on a C57Bl/6 background. Syndecan-4 deficient mice were obtained from Dr. Tetsuhito Kojima, Nagoya University, Japan (Ishiguro et al., 2000). *Ccr7*$^{-/-}$ mice (Forster et al., 1999) and *Rosa* reporter mice were from Jackson Laboratory. *Ext1*$^{flox/flox}$ line was generated as reported (Inatani et al., 2003). *Tet-Cre* line was provided by Dr. Andras Nagy (Belteki et al., 2005). The generation *Tek-rtTA* transgenic mice and their husbandry with *Tet-Cre* and *Ext1*$^{flox/flox}$ mice are described in Supplemental Experimental Procedure. Mice were treated according to guidelines of the National Institutes of Health, and experiments were approved by the Animal Research Committee of the Sanford-Burnham Medical Research Institute.

Dendritic cell homing

In vitro culture of bone marrow-derived dendritic cells and their homing to inflamed draining lymph nodes was performed as described (Inaba et al., 1992; Sangaletti et al., 2005). Briefly, bone marrow cells were obtained from the thigh bones of WT mice and cultured with RPMI medium containing 5% FBS, 5 ng/ml of mouse GM-CSF and 10 ng/ml of mouse IL-4 at 37°C in a humid incubator. On day 3 and day 5, half of the culture medium was replaced with the same volume of fresh medium containing cytokines as described above. On day 7, loosely attached cells were harvested by pipeting and incubated with CD11c antibody. CD11c^{+} cells were isolated by magnet-assisted cell sorting (MACS) beads conjugated with anti-rat IgG and a MACS LS column (Miltenyi Biotec GmbH). Isolated cells were labeled with 5-chloromethylfluorescein (CMFDA) and injected intradermally into shaved mouse abdomen skin (5×10^5 cells per mouse). After 30 min, 25 μl of 0.5% of DNFB was applied to the shaved mouse abdomen skin. Twenty four hours later, the draining inguinal lymph nodes were dissected and dissociated into single cell suspension. Cells were subjected to cell number analysis using a cytometer and stained with PE-conjugated CD11c antibody on ice, followed by flow cytometric analysis of the fractional content of CD11c^{+} and CMFDA^{+} double positive cells. Homing of exogenous dendritic cells were calculated by multiplying total cell number of draining lymph nodes with fractional content of double positive cells as described above.

Intravital Microscopy and Image Analysis

Intravital microscopy of inguinal LNs was performed as previously described (Warnock et al., 1998 and M'rini et al., 2003). Briefly, control or mutant mice were anesthetized and the right inguinal LN was exposed and positioned for epifluorescence intravital microscopy. Preparations were transferred to an intravital microscope (IV-500; Mikron Instruments, San Diego, CA), equipped with a Rapp OptoElectronic SP-20 xenon flash lamp system (Hamburg, Germany) and QImaging Rolera-MGi EMCCD camera (Surrey, BC). T cells were isolated from the spleens and LNs from naïve WT mice using pan T cell isolation kits (Miltenyi Biotec). T cells were fluorescently labeled with 1 ng/mL calcein-AM for 20

minutes at 37°C, and small boluses (10–50 μL of 10×10^6 cells/mL) of cells were injected via a left femoral artery catheter. Cell behavior in LN venules was recorded in 10-minute recordings through 10× or 20× water-immersion objectives (Achroplan; Carl Zeiss). Rolling and sticking fractions in individual vessel segments were determined off-line by playback of digital video files. Rolling fraction was determined as the percentage of cells interacting with LN venules in the total number of cells passing through a vessel during the observation period. Sticking fraction was defined as the percentage of rolling cells that adhered in LN venules for 30 or more seconds. V_{roll} was defined as the mean velocity (μm/s) of rolling cells and V_{fast} as the mean velocity of noninteracting cells in each vessels. The highest velocity, V_{max}, was used to calculate the mean blood flow velocity, Vblood, using the relation: $V_{blood} = V_{max}/(1.6- E\text{^}2)$ where E is the ratio of the leukocyte diameter (as assumed to be 7 μm) to vessel diameter, as previously published (Ley and Gaehtgens, 1991). The wall shear rate (WSR) was assessed as: $WSR = V_{blood}*8/D_v$ were D_v is the vessel diameter. A cumulative velocity curve was compiled by plotting the percentage of rolling cells at or below a given velocity as a function of V_{roll}. Rolling fraction and velocities were determined in identical venules for each condition. Statistic difference was evaluated by unpaired t test.

Supplementary Material

Refer to Web version on PubMed Central for supplementary material.

Acknowledgments

We thank Drs. M. N. Fukuda and F. Ire for support and advice; Drs. S. Rosen, T. Sato and T. Kojima and A. Nagy for 38C13 cells, Tie2-promoter plus enhancer, syndecan-4 deficient mice and *Tet-Cre* mice, respectively; L. Wang, B. Charbono, Y. Altman, J. Tomlin, P. Lee, L. Haynes and G. Chen for technical assistance; Dr. E. Lamar for critical reading of the manuscript; and A. Morse for organizing the manuscript. This work was supported by National Institute of Health grant PO1 CA71932 to M.F., U.H.v.A., and J.L, NIH T32 Training Grant in Hematology (E.A.M), and Toyobo Biotechnology Fellowship (Y.I.).

References

Arbones ML, Ord DC, Ley K, Ratech H, Maynard-Curry C, Otten G, Capon DJ, Tedder TF. Lymphocyte homing and leukocyte rolling and migration are impaired in L-selectin-deficient mice. Immunity. 1994; 1:247–260. [PubMed: 7534203]

Bajenoff M, Egen JG, Koo LY, Laugier JP, Brau F, Glaichenhaus N, Germain RN. Stromal cell networks regulate lymphocyte entry, migration, and territoriality in lymph nodes. Immunity. 2006; 25:989–1001. [PubMed: 17112751]

Belteki G, Haigh J, Kabacs N, Haigh K, Sison K, Costantini F, Whitsett J, Quaggin SE, Nagy A. Conditional and inducible transgene expression in mice through the combinatorial use of Cre-mediated recombination and tetracycline induction. Nucleic Acids Res. 2005; 33:e51. [PubMed: 15784609]

Bishop JR, Schuksz M, Esko JD. Heparan sulphate proteoglycans fine-tune mammalian physiology. Nature. 2007; 446:1030–1037. [PubMed: 17460664]

Butcher EC, Picker LJ. Lymphocyte homing and homeostasis. Science. 1996; 272:60–66. [PubMed: 8600538]

Cyster JG, Shotton DM, Williams AF. The dimensions of the T lymphocyte glycoprotein leukosialin and identification of linear protein epitopes that can be modified by glycosylation. EMBO J. 1991; 10:893–902. [PubMed: 1706994]

David G, Bai XM, Van der Schueren B, Cassiman JJ, Van den Berghe H. Developmental changes in heparan sulfate expression: in situ detection with mAbs. J Cell Biol. 1992; 119:961–975. [PubMed: 1385449]

Ellies LG, Tsuboi S, Petryniak B, Lowe JB, Fukuda M, Marth JD. Core 2 oligosaccharide biosynthesis distinguishes between selectin ligands essential for leukocyte homing and inflammation. Immunity. 1998; 9:881–890. [PubMed: 9881978]

Forster R, Schubel A, Breitfeld D, Kremmer E, Renner-Muller I, Wolf E, Lipp M. CCR7 coordinates the primary immune response by establishing functional microenvironments in secondary lymphoid organs. Cell. 1999; 99:23–33. [PubMed: 10520991]

Garner OB, Yamaguchi Y, Esko JD, Videm V. Small changes in lymphocyte development and activation in mice through tissue-specific alteration of heparan sulphate. Immunology. 2008; 125:420–429. [PubMed: 18479348]

Homeister JW, Thall AD, Petryniak B, Maly P, Rogers CE, Smith PL, Kelly RJ, Gersten KM, Askari SW, Cheng G, et al. The alpha(1,3)fucosyltransferases FucT-IV and FucT-VII exert collaborative control over selectin-dependent leukocyte recruitment and lymphocyte homing. Immunity. 2001; 15:115–126. [PubMed: 11485743]

Inaba K, Inaba M, Romani N, Aya H, Deguchi M, Ikehara S, Muramatsu S, Steinman RM. Generation of large numbers of dendritic cells from mouse bone marrow cultures supplemented with granulocyte/macrophage colony-stimulating factor. J Exp Med. 1992; 176:1693–1702. [PubMed: 1460426]

Inatani M, Irie F, Plump AS, Tessier-Lavigne M, Yamaguchi Y. Mammalian brain morphogenesis and midline axon guidance require heparan sulfate. Science. 2003; 302:1044–1046. [PubMed: 14605369]

Ishiguro K, Kadomatsu K, Kojima T, Muramatsu H, Tsuzuki S, Nakamura E, Kusugami K, Saito H, Muramatsu T. Syndecan-4 deficiency impairs focal adhesion formation only under restricted conditions. J Biol Chem. 2000; 275:5249–5252. [PubMed: 10681494]

Kansas GS. Selectins and their ligands: current concepts and controversies. Blood. 1996; 88:3259–3287. [PubMed: 8896391]

Kawashima H, Petryniak B, Hiroka N, Mitoma J, Huckaby V, Nakayama J, Uchimura K, Kadomatsu K, Miuramatsu T, Lowe JB, et al. N-acetylglucosamine-6-O-sulfotransferases 1 and 2 cooperatively control lymphocyte homing through L-selectin ligand biosynthesis in high endothelial venules. Nat Immunol. 2005; 6:1096–1104. [PubMed: 16227985]

Koni PA, Joshi SK, Temann UA, Olson D, Burkly L, Flavell RA. Conditional vascular cell adhesion molecule 1 deletion in mice: impaired lymphocyte migration to bone marrow. J Exp Med. 2001; 193:741–754. [PubMed: 11257140]

Kriehuber E, Breiteneder-Geleff S, Groeger M, Soleiman A, Schoppmann SF, Stingl G, Kerjaschki D, Maurer D. Isolation and characterization of dermal lymphatic and blood endothelial cells reveal stable and functionally specialized cell lineages. J Exp Med. 2001; 194:797–808. [PubMed: 11560995]

Lander AD, Nie Q, Wan FY. Do morphogen gradients arise by diffusion? Dev Cell. 2002; 2:785–796. [PubMed: 12062090]

Ley K, Gaehtgens P. Endothelial, not hemodynamic, differences are responsible for preferential leukocyte rolling in rat mesenteric venules. Circ, Res. 1991; 69:1034–1041. [PubMed: 1934331]

Lortat-Jacob H, Grosdidier A, Imberty A. Structural diversity of heparan sulfate binding domains in chemokines. Proc Natl Acad Sci U S A. 2002; 99:1229–1234. [PubMed: 11830659]

Massena S, Christoffersson G, Hjertstrom E, Zcharia E, Vlodavsky I, Ausmees N, Rolny C, Li J-P, Phillipson M. A chemotactic gradient sequestered on endothelial heparan sulfate induces directional intraluminal crawling of neutrophils. Blood. (In press).

M'Rini C, Cheng G, Schweitzer C, Cavanagh LL, Palframan RT, Mempel TR, Warnock RA, Lowe JB, Quackenbush EJ, von Andrian UH. A novel endothelial L-selectin ligand activity in lymph node medulla that is regulated by alpha(1,3)-fucosyltransferase-IV. J Exp Med. 2003; 198:1301–1312. [PubMed: 14597733]

Marchesi VT, Gowans JL. The Migration of Lymphocytes through the Endothelium of Venules in Lymph Nodes: An Electron Microscope Study. Proc R Soc Lond B Biol Sci. 1964; 159:283–290. [PubMed: 14114164]

McEver RP, Zhu C. Rolling cell adhesion. Annu Rev Cell Dev Biol. 2010; 26:7.1–7.34.

Middleton J, Neil S, Wintle J, Clark-Lewis I, Moore H, Lam C, Auer M, Hub E, Rot A. Transcytosis and surface presentation of IL-8 by venular endothelial cells. Cell. 1997; 91:385–395. [PubMed: 9363947]

Mitoma J, Bao X, Petryanik B, Schaerli P, Gauguet JM, Yu SY, Kawashima H, Saito H, Ohtsubo K, Marth JD, et al. Critical functions of N-glycans in L-selectin-mediated lymphocyte homing and recruitment. Nat Immunol. 2007; 8:409–418. [PubMed: 17334369]

Nakano H, Mori S, Yonekawa H, Nariuchi H, Matsuzawa A, Kakiuchi T. A novel mutant gene involved in T-lymphocyte-specific homing into peripheral lymphoid organs on mouse chromosome 4. Blood. 1998; 91:2886–2895. [PubMed: 9531599]

Parish CR. The role of heparan sulphate in inflammation. Nat Rev Immunol. 2006; 6:633–643. [PubMed: 16917509]

Phan UT, Waldron TT, Springer TA. Remodeling of the lectin-EGF-like domain interface in P- and L-selectin increases adhesiveness and shear resistance under hydrodynamic force. Nat Immunol. 2006; 7:883–889. [PubMed: 16845394]

dePaz JL, Moseman EA, Noti C, Polito L, von Andrian UH, Seeberger PH. Profiling heparin-chemokine interactions using synthetic tools. ACS Chem Biol. 2007; 2:735–744. [PubMed: 18030990]

Rosen SD. Ligands for L-selectin: homing, inflammation, and beyond. Annu Rev Immunol. 2004; 22:129–156. [PubMed: 15032576]

Sangaletti S, Gioiosa L, Guiducci C, Rotta G, Rescigno M, Stoppacciaro A, Chiodoni C, Colombo MP. Accelerated dendritic-cell migration and T-cell priming in SPARC-deficient mice. J Cell Sci. 2005; 118:3685–3694. [PubMed: 16046482]

Schlaeger TM, Bartunkova S, Lawitts JA, Teichmann G, Risau W, Deutsch U, Sato TN. Uniform vascular-endothelial-cell-specific gene expression in both embryonic and adult transgenic mice. Proc Natl Acad Sci USA. 1997; 94:3058–3063. [PubMed: 9096345]

Schumann K, Lammermann T, Brucker M, Legler DF, Polleux J, Spatz JP, Schuler G, Forster R, Lutz MB, Sorokin L, et al. Immobilized chemokine fields and soluble chemokine gradients cooperatively shape migration patterns of dendritic cells. Immunity. 2010; 32:703–713. [PubMed: 20471289]

Shamri R, Grabovsky V, Gauguet JM, Feigelson S, Manevich E, Kolanus W, Robinson MK, Staunton DE, von Andrian UH, Alon R. Lymphocyte arrest requires instantaneous induction of an extended LFA-1 conformation mediated by endothelium-bound chemokines. Nat Immunol. 2005; 6:497–506. [PubMed: 15834409]

Shimaoka M, Xiao T, Liu JH, Yang Y, Dong Y, Jun CD, McCornmack A, Zhang R, Joachimiak A, Takagi J, et al. Structures of the alpha L I domain and its complex with ICAM-1 reveal a shape-shifting pathway for integrin regulation. Cell. 2003; 112:99–111. [PubMed: 12526797]

Shimoda H. Immunohistochemical demonstration of Angiopoietin-2 in lymphatic vascular development. Histochem Cell Biol. 2009; 131:231–238. [PubMed: 18836739]

Springer TA. Traffic signals for lymphocyte recirculation and leukocyte emigration: the multistep paradigm. Cell. 1994; 76:301–314. [PubMed: 7507411]

Staite ND, Justen JM, Sly LM, Beaudet AL, Bullard DC. Inhibition of delayed-type contact hypersensitivity in mice deficient in both E-selectin and P-selectin. Blood. 1996; 88:2973–2979. [PubMed: 8874194]

Subramaniam M, Saffaripour S, Watson SR, Mayadas TN, Hynes RO, Wagner DD. Reduced recruitment of inflammatory cells in a contact hypersensitivity response in P-selectin-deficient mice. J Exp Med. 1995; 181:2277–2282. [PubMed: 7539046]

Uchimura K, Gauguet JM, Singer MS, Tsay D, Kannagi R, Muramatsu T, von Andrian UH, Rosen SD. A major class of L-selectin ligands is eliminated in mice deficient in two sulfotransferases expressed in high endothelial venules. Nat Immunol. 2005; 6:1105–1113. [PubMed: 16227986]

van Zante A, Gauguet JM, Bistrup A, Tsay D, von Andrian UH, Rosen SD. Lymphocyte-HEV interactions in lymph nodes of a sulfotransferase-deficient mouse. J Exp Med. 2003; 198:1289–1300. [PubMed: 14597732]

von Andrian UH, Mempel TR. Homing and cellular traffic in lymph nodes. Nat Rev Immunol. 2003; 3:867–878. [PubMed: 14668803]

Wang L, Fuster M, Sriramarao P, Esko JD. Endothelial heparan sulfate deficiency impairs L-selectin- and chemokine-mediated neutrophil trafficking during inflammatory responses. Nat Immunol. 2005; 6:902–910. [PubMed: 16056228]

Warnock A, Askari S, Butcher EC, von Andrian UH. Molecular mechanisms of lymphocyte homing to peripheral lymph nodes. J Exp Med. 1998; 187:205–216. [PubMed: 9432978]

Yang BG, Tanaka T, Jang MH, Bai Z, Hayasaka H, Miyasaka M. Binding of lymphoid chemokines to collagen IV that accumulates in the basal laminina of high endothelial venules:its implications in lymphocyte trafficking. J Immunol. 2007; 179:4376–4382. [PubMed: 17878332]

Yeh JC, Hiraoka N, Petryniak B, Nakayama J, Ellies LG, Rabuka D, Hindsgaul O, Marth JD, Lowe JB, Fukuda M. Novel sulfated lymphocyte homing receptors and their control by a Core1 extension β1,3-N-acetylglucosaminyltransferase. Cell. 2001; 105:957–969. [PubMed: 11439191]

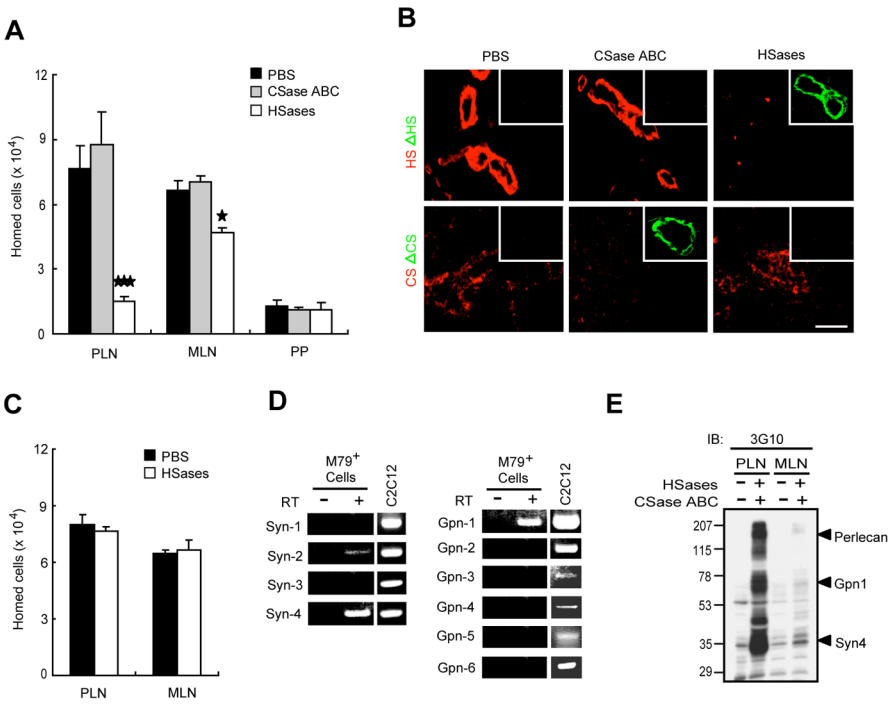

Figure 1.

Diminished lymphocyte homing upon enzymatic removal of endothelial heparan sulfate. (**A**) Homing of labeled WT lymphocytes to lymph nodes of enzyme-infused WT mice. Chondroitinase ABC (CSase ABC) or a mixture of heparitinase and heparinase (HSases) in PBS was injected through mouse tail veins 2 hr before cell injection (n = 3–5). PBS was infused as a control. *, $P < 0.05$; ***, $P < 0.001$, versus PBS. (**B**) Immunostaining of lymph node frozen sections. Monoclonal antibodies (mAbs) 10E4 and 3G10 detected intact heparan sulfate and digested HS proteoglycans (ΔHS), respectively, while mAbs CS56 and 2B6 stained chondroitin sulfate and digested CS proteoglycans (ΔCS), respectively. *Bar*, 50 μm. (**C**) Homing of HSase-treated and labeled lymphocytes from WT mice to the lymph nodes of WT mice. PBS treatment was run as a control. (**D**) RT-PCR analysis of membrane-associated heparan sulfate proteoglycans in isolated MECA-79$^+$ cells from WT mice and a control mouse myoblast cell line C2C12. (**E**) Immune blot of lymph node vascular heparan sulfate proteoglycans. Matrix of lymph nodes from the WT mice that received Hsases and CSase ABC was solubilized with Triton X-100-containing buffer, separated by SDS-PAGE and blotted with mAb 3G10. Equal amounts of proteins were loaded on each lane. The migration position of perlecan, glypican-1 (Gpn1) and syndecan-4 (Syn4) are indicated. Data in A and C are representative of four independent experiments (mean ± S.E.).

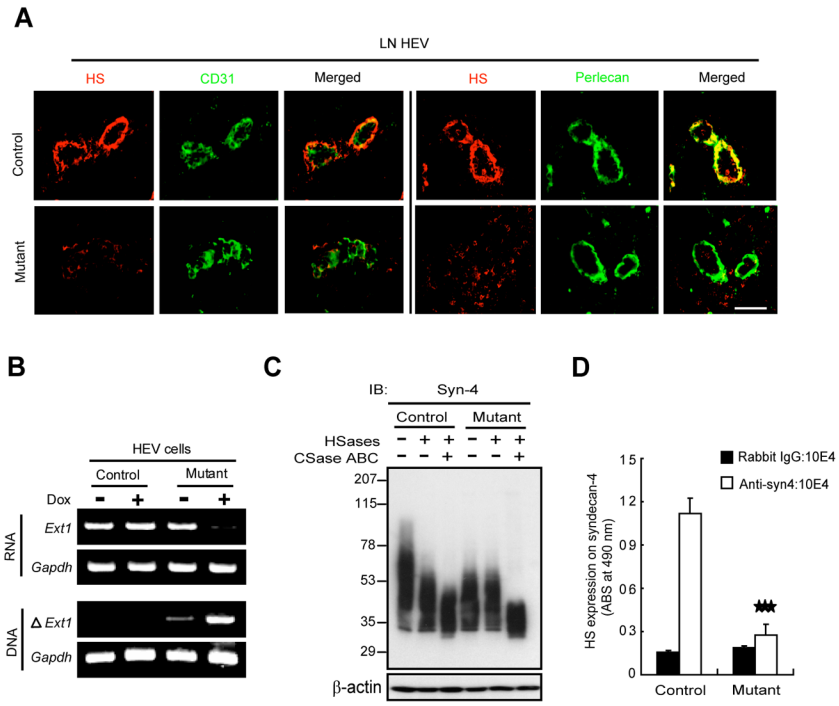

Figure 2.

Inducible abrogation of endothelial heparan sulfate in *Ext1* mutant mice. (**A**) Immunostaining of high endothelial venule (HEV) heparan sulfate in frozen lymph node (LN) sections by mAb 10E4. Co-staining with CD31 or perlecan was performed. *Bar*, 50 μm. (**B**) Analysis of PCR products of *Ext1* in HEV cells isolated from the control and mice. Δ*Ext1* denotes deficient *Ext1* gene. (**C**) Immune blot of syndecan-4 (Syn-4) in lung endothelial cells isolated from control and mutant mice. Pretreatment with a mixture of heparitinase and heparinase (Hsases) and/or chondroitinase ABC (CSase ABC) at 37°C for 1 hr was included. (**D**) ELISA of heparan sulfate chains on syndencan-4 or control (IgG) immunoprecipitate from lung endothelial cells of the control and mutant mice by using mAb 10E4. Data are expressed as mean ± S.D..

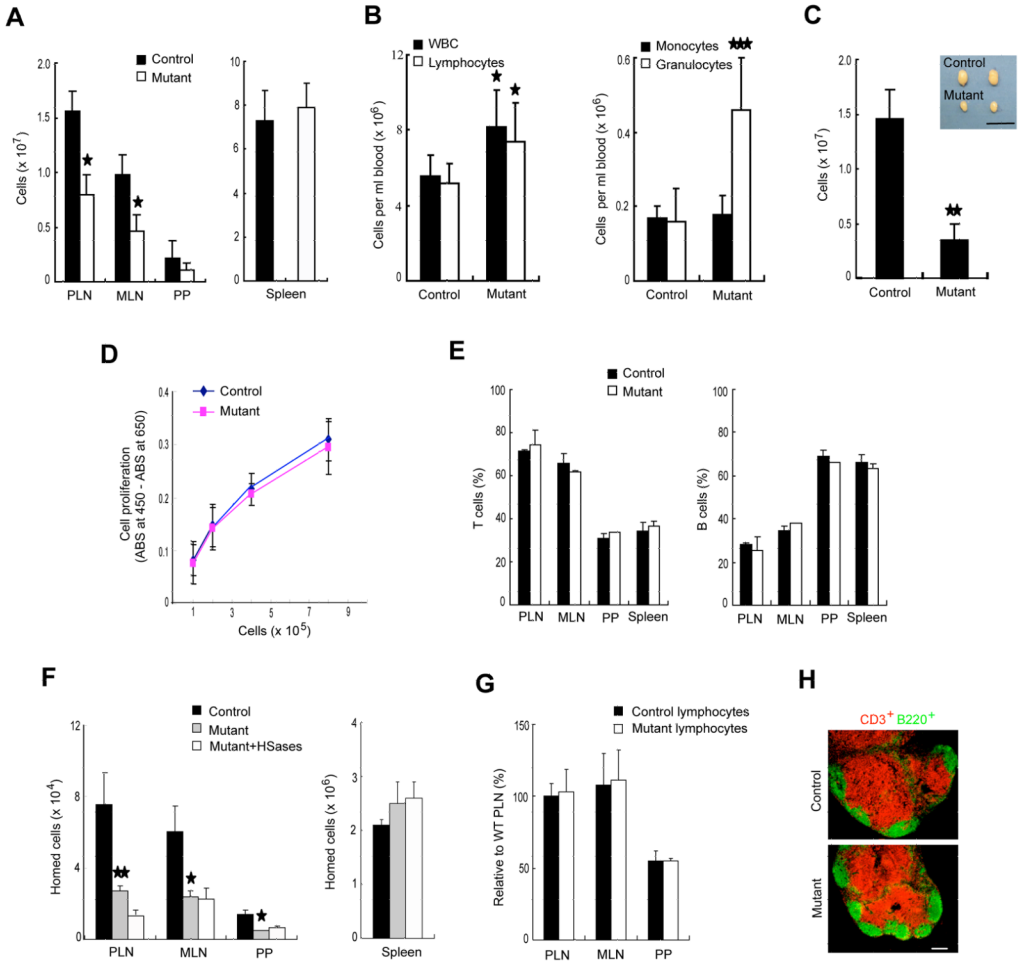

Figure 3.

Impaired lymphocyte homing and lymph node cellularity in *Ext1* mutant mice. (**A**) Cell numbers of secondary lymphoid organs in mice that received doxycycline for 3–4 weeks (n = 5–9). (**B**) Numbers of white blood cells (WBC) and subtypes in the peripheral blood of the mice after 4 weeks treatment with doxycyline (n = 8). (**C**) Cell numbers of PLNs in the mice that received doxycycline for 2 months (n = 4–6). Insert shows the visual size of the representative inguinal lymph nodes from both mouse lines. *Bar*, 0.5 cm. (**D**) Proliferation of lymph node cells stimulated by Concanavalin A at a dose of 2 μg/ml. (**E**) Populations of T cells ($CD3^+$) and B cells ($B220^+$) in secondary lymphoid organs. (**F**) Homing of labeled lymphocytes from WT mice to the secondary lymphoid organs of the control and the mutant mice (n = 3–5). An infusion of heparitinase and heparinase (HSases) was included for the mutant mice. (**G**) Homing of labeled lymphocytes isolated from the control or the mutant mice to the lymph nodes of WT mice (n = 3–5). (**H**) Immunostaining of lymph node sections with anti-CD3 (in red) and anti-B220 (in green). *Bar*, 200 μm. *, $P < 0.05$; **, $P < 0.01$, versus controls. Data are representative of two or three independent experiments (mean ± S.E.).

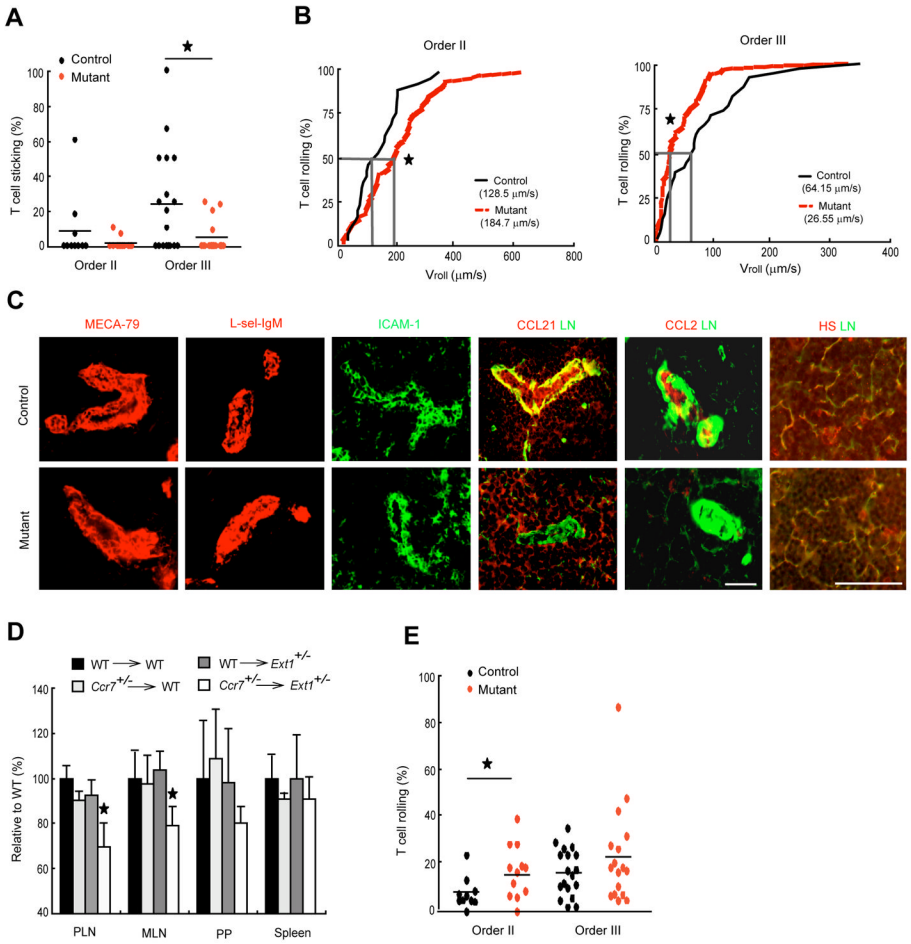

Figure 4.

Diminished sticking and decreased rolling velocity of lymphocytes in *Ext1* mutant mice. (**A**) Sticking fraction of T cells in orders II and III lymph node venules analyzed by intravital microscopy. Combined results of 6–7 venules for order II and 13 venules for order III from 8 mice of each group are shown. (**B**) Cumulative rolling velocity of T cells in orders II and III lymph node venules of control and mutant mice (n = 8). The percentage of rolling cells is expressed as function of V_{roll} (see Experimental Procedures). (**C**) Immunostaining of MECA-79 antigen (MECA-79), L-selectin ligands (L-sel-IgM), intercellular adhesion molecule-1 (ICAM-1), chemokines CCL21 and CCL2, and laminin (LN) in lymph node frozen sections. *Bars*, 50 μm. (**D**) Homing of labeled lymphocytes isolated from WT or $Ccr7^{+/-}$ mice to the lymph nodes of WT mice or $Ext1^{+/-}$ mice (n = 4). (**E**) Rolling fraction of T cells in orders II and III lymph node venules analyzed by intravital microscopy. Combined results of 6–7 venules for order II and 13 venules for order III from 8 mice of each group are shown. Mean values are shown as horizontal bars in A and E. *, $P < 0.05$, versus control mice (unpaired t test).

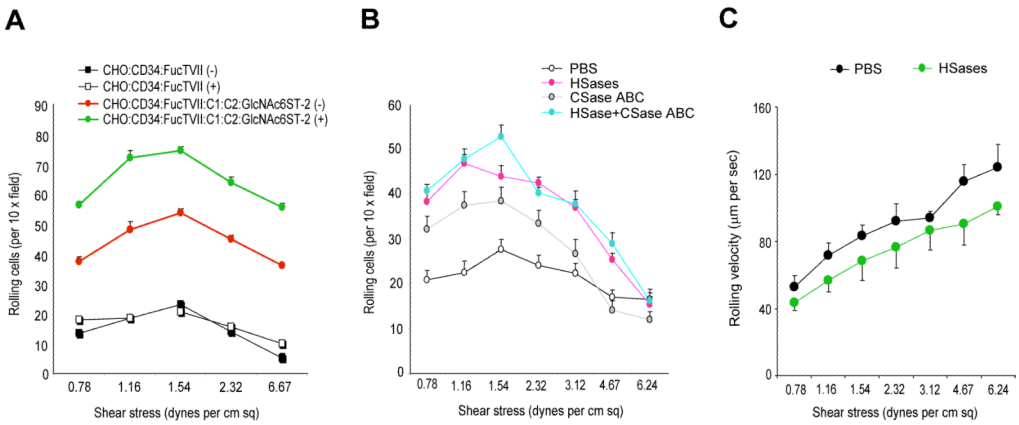

Figure 5.

Rolling of 38C13 cells on CHO cells expressing 6-sulfo sLe^X or sLe^X on *N*-glycans and *O*-glycans. (**A**) Rolling of 38C13 cells on CHO cells expressing 6-sulfo sLe^X on both *N*- and *O*-glycans (CHO:CD34:FucT-VII:C1:C2:GlcNAc6ST-2) or on CHO cells expressing only *N*-glycans sLe^X (CHO:CD34:FucT-VII) without enzyme treatment (−) or treated with chondroitinase ABC (CSase ABC), heparitinase and heparinase (HSases) (+). (**B**) Cell rolling on CHO cells expressing 6-sulfo sLe^X on both *N*- and *O*-glycans treated with individual enzyme described in A. (**C**) Rolling velocity on PBS- or HSase-treated CHO cells expressing 6-sulfo sLe^X as shown in B. Data are representative of two independent experiments (mean ± S.E.).

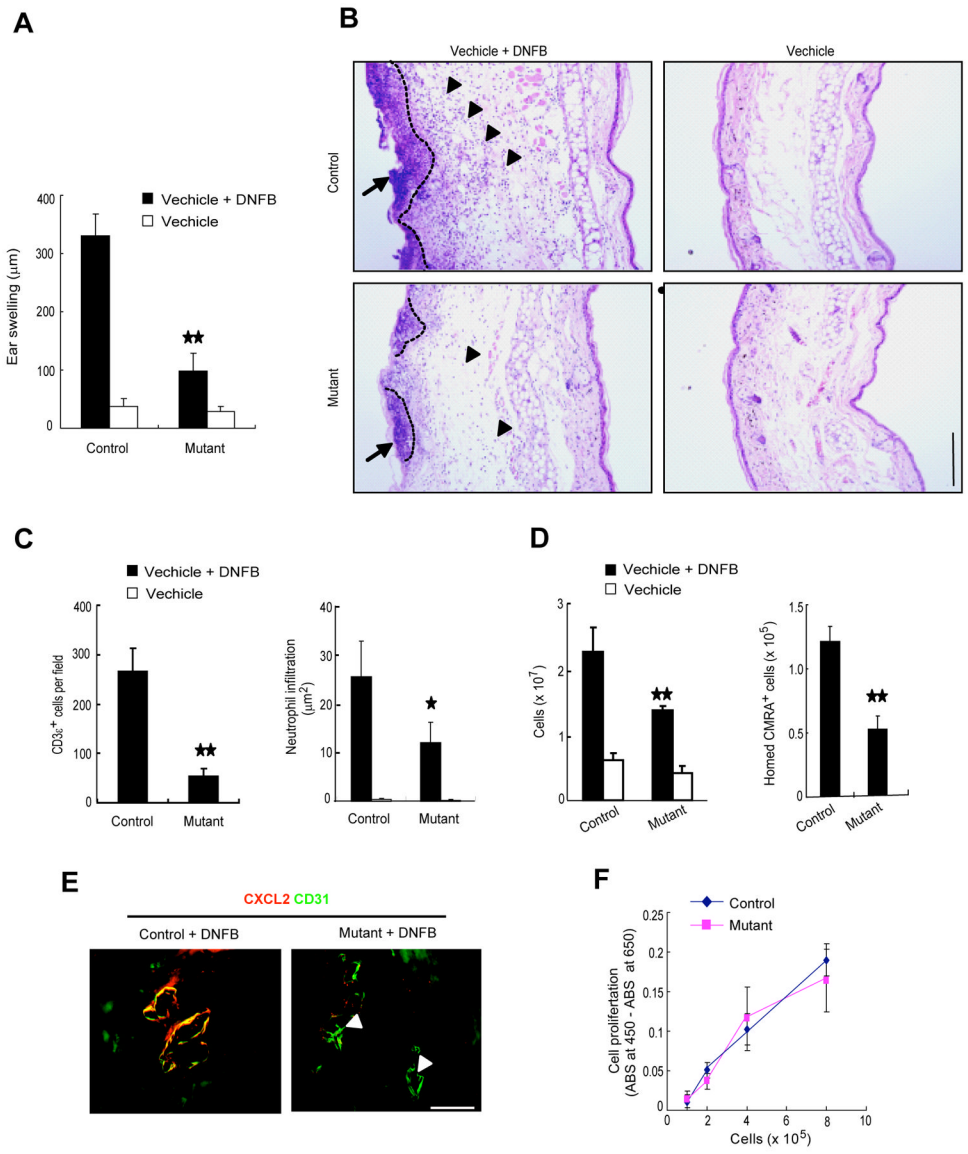

Figure 6.

Impaired contact hypersensitivity in *Ext1* mutant mice. (**A**) Ear swelling 24 hr after challenge with DNFB or vehicle alone in control and mutant mice (n = 4–6). (**B**) Hematoxylin and eosin staining of ear sections challenged with DNFB. Arrowheads are infiltrated mononuclear cells; arrows are infiltrated neutrophils; dashed areas are epidermal areas with neutrophil clustering. *Bar*, 250 μm. (**C**) Quantitation of infiltrated T cells in inflamed ears (left panels) and areas of neutrophil clusters (right panels) (n = 3–5). Numbers of CD3ε$^+$ cells in the area of 300 μm long ear were counted, while the epidermis area with clustered neutrophils of the whole ear were measured. (**D**) Cell number of sensitized draining inguinal lymph nodes (left panels) and lymphocyte homing to the draining inguinal lymph nodes (right panels) (n= 3–5). (**E**) CXCL2 expression in CD31$^+$ cells of DNFB-inflamed abdominal skins. Arrowheads indicate microvessels. *Bar*, 25 μm. (**F**) Cell proliferation isolated from sensitized inguinal lymph nodes in response to DNBS (200 μg/ml) (n= 3). *, $P < 0.05$; **, $P < 0.01$, versus control mice. Data are representative of two independent experiments (mean ± S.E.)

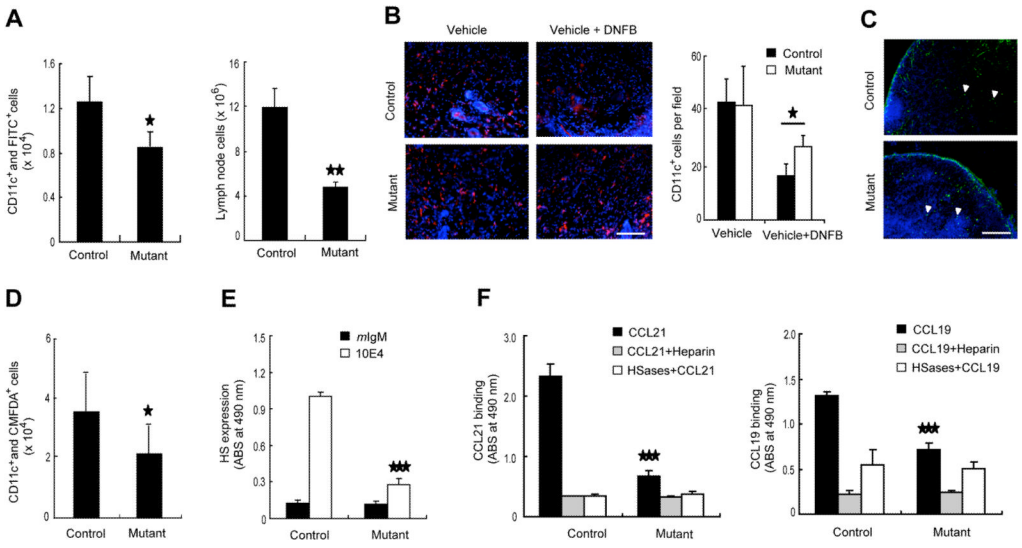

Figure 7.

Impaired migration of dendritic cells to lymph nodes in *Ext1* mutant mice. (**A**) Cell numbers of draining lymph nodes (right panels) and homing of dendritic cells to draining lymph nodes (left panels) in skin painting experiment (n = 4–5). (**B**) Immunofluorescent staining of resident dendritic cells (red) in DNFB-inflamed skin epidermis. Nuclei (blue) were stained by Hoechst. *Bar*, 100 μm. (**C**) Immunofluorescence of draining lymph nodes in skin painting experiments. Arrowheads point to infiltrated FITC-bearing dendritic cells. *Bar*, 200 μm. (**D**) Homing of intrademally loaded dendritic cells to draining lymph nodes (n = 3–5). (**E**) ELISA of heparan sulfate expression assessed by mAb 10E4 in cultured mouse skin lymphatic endothelial cells. (**F**) Binding of recombinant mouse CCL21 or CCL19 to cultured skin lymphatic endothelial cells. In some cases, addition of heparin (100 μg/ml) or a pretreatement with heparitinase and heparinase (HSases) at 37 °C for 1 h was included. *, $P < 0.05$; **, $P < 0.01$; ***, $P < 0.001$ versus control mice. Data are expressed as mean ± S.E. for A, B and D, and mean ± S.D. for E and F.